JCTC Journal of Chemical Theory and Computation

Article

pubs.acs.org/JCTC

Hierarchical Biomolecular Dynamics: Picosecond Hydrogen Bonding Regulates Microsecond Conformational Transitions

Sebastian Buchenberg,[†] Norbert Schaudinnus,[†] and Gerhard Stock*[,†,‡]

[†]Biomolecular Dynamics, Institute of Physics, Albert Ludwigs University, Freiburg, 79104 Germany

[‡]Freiburg Institute for Advanced Studies (FRIAS), Albert Ludwigs University, Freiburg, 79104 Germany

Supporting Information

ABSTRACT: Biomolecules exhibit structural dynamics on a number of time scales, including picosecond (ps) motions of a few atoms, nanosecond (ns) local conformational transitions, and microsecond (μs) global conformational rearrangements. Despite this substantial separation of time scales, fast and slow degrees of freedom appear to be coupled in a nonlinear manner; for example, there is theoretical and experimental evidence that fast structural fluctuations are required for slow functional motion to happen. To elucidate a microscopic mechanism of this multiscale behavior, Aib peptide is adopted as a simple model system. Combining extensive molecular dynamics simulations with principal component analysis techniques, a hierarchy of (at least) three tiers of the molecule's free energy landscape is discovered. They correspond to chiral left- to right-handed transitions of the entire peptide that happen on a μs time scale, conformational transitions of individual residues that take about 1 ns, and the opening and closing of structure-stabilizing hydrogen bonds that occur within tens of ps and are triggered by sub-ps structural fluctuations. Providing a simple mechanism of hierarchical dynamics, fast hydrogen bond dynamics is found to be a prerequisite for the ns local conformational transitions, which in turn are a prerequisite for the slow global conformational rearrangement of the peptide. As a consequence of the hierarchical coupling, the various processes exhibit a similar temperature behavior which may be interpreted as a dynamic transition.

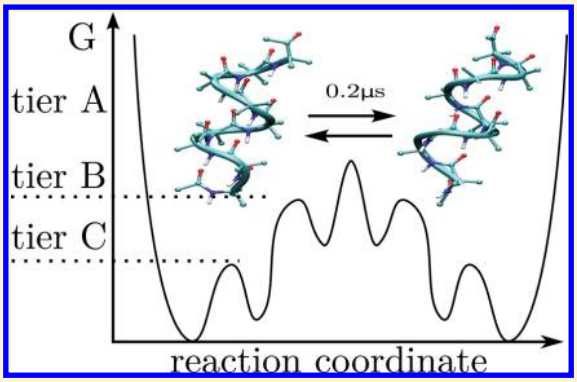

INTRODUCTION

Multiscale processes that occur on several length- and time-scales are ubiquituous in such diverse areas as geophysics, material science, system biology, and biophysics.[1] For example, biomolecular systems such as proteins in aqueous solution exhibit nuclear motion on a multitude of time scales, ranging from localized bond vibrations within tens of femtoseconds and picosecond (ps) dynamics of low-frequency normal modes to nanosecond (ns) local conformational transitions and large conformational rearrangements occurring on a microsecond (μs) time scale or even longer.[2] Driven by recent experimental and computational progress, this structural dynamics has been recognized as an essential player for the functionality of proteins.[3−7] The importance of functional dynamics (e.g., in folding, aggregation, binding and signaling) extends the classic structure−function paradigm of biochemistry to include the "dynamical personality" of proteins.[3] It also gave rise to the notion of the dynasome,[7] which suggests that—apart from the structure—the dynamical properties of proteins are evolutionarily conserved.

The mere existence of multiple time scales in molecular dynamics is easy to understand. Employing a normal-mode analysis to calculate the eigenfrequencies of the system, we identify fast modes as local vibrations of a few atoms and slow modes as global motions of the molecule involving many atoms.[8] In the harmonic approximation, these normal modes are independent. More generally, one often assumes that motions occurring on different time scales can be separated and thus treated as uncoupled (e.g., the "adiabatic" picture of fast electrons instantaneously following slow nuclei).[2] In many important cases, however, fast and slow degrees of freedom are coupled in an anharmonic and nonadiabatic manner. For example, it is known that the neglect of fast degrees of freedom in molecular dynamics (MD) simulations (e.g., by constraining internal motions[9] or using implicit solvent models and coarse-grained representations[10,11]) may significantly change the dynamics of the slow degrees of freedom. On the experimental side, nuclear magnetic resonance relaxation studies have reported increased ps/ns fluctuations of functional protein residues that undergo μs conformational transitions.[12,13] These examples of multiscale dynamics (i.e., coupled dynamics on several time scales) suggest that fast fluctuations may be a prerequisite of slow functional dynamics.

Multiscale dynamics is often illustrated by a "hierarchical" free energy landscape;[14−16] see Figure 1a. Representing the free energy in terms of some reaction coordinate, the energy landscape is characterized by its minima (which represent the

Received: December 19, 2014
Published: February 11, 2015

DOI: 10.1021/ct501156t
J. Chem. Theory Comput. 2015, 11, 1330−1336

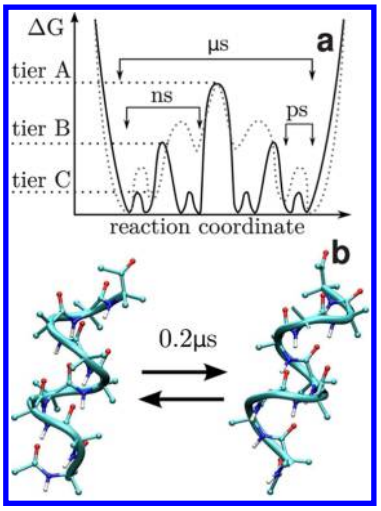

Figure 1. (a) General scheme of a hierarchical free energy landscape that represents dynamical processes on different time scales (ps, ns, and μs) by various tiers (C, B, and A). The separation of time scales can be caused by different barrier heights (full line) or by a sequential reaction involving high back-rates (dotted line). (b) The achiral peptide Aib_9 undergoes transitions between left- and right-handed helices on a microsecond time scale (tier A). While the slowest motions of the system often account for its biological function, the underlying fast dynamics (tiers B and C) may be elusive.

metastable conformational states of the system) and its barriers (which connect these states).[17−23] The effects of the solvent and the many remaining molecular coordinates not included in this low-dimensional picture is usually approximated in terms of a diffusion process.[20,24] A hierarchical free energy landscape, in particular, represents the dynamics on different time scales by various tiers of the energy landscape, associating, for example, tiers C, B, and A with specific processes on a ps, ns, and μs time scale, respectively. The notion of a hierarchy implies that these processes interact such that the fast processes regulate the slow transitions. Notably, the restriction to a low-dimensional reaction coordinate in Figure 1a appears to suggest a simple coupling between fast and slow motions. For example, one needs to cross the barriers in tier C to reach the barriers of tier B. While the hierarchical energy landscape model has been designed to account for such phenomena, so far it has served more as a general concept rather than a practical approach to explain the multiscale dynamics of a specific protein. Hence, the goal of this paper is to identify the coupled fast and slow motions for a simple but nontrivial model example and to gain a detailed understanding of the microscopic mechanism underlying the hierarchical dynamics.

With this end in mind, we reconsider recent experimental and computational studies on the 'dynamic transition' of a short 3_{10} peptide helix.[25−27] Employing time-resolved vibrational spectroscopy to study photoinduced energy transport through a Aib_9 peptide in chloroform, Hamm and co-workers found that the homogeneous dephasing rate of the C=O vibrations as well as the overall transport efficiency stays approximately constant from 220−260 K, but rises steeply for higher temperatures. Both experimental observables report on ps dynamics of the peptide. Complementary MD simulations showed a prominent rise of the atomic fluctuations of the peptide at 270 K.[28,29] Because the latter occur on a ns time scale, however, it remained unclear how the ns conformational dynamics may affect the ps observables of homogeneous broadening and energy transport.

This work aims to elucidate this finding and study its relation to hierarchical dynamics. To this end, we perform extensive MD simulations of Aib peptide at various temperatures from 200 to 350 K, collecting, in total, ≈200 μs simulation time. Using systematic dimensionality reduction techniques,[30−34] we identify a hierarchy of three tiers corresponding to dynamics on a time scale of ps, ns, and μs. Being an achiral peptide, Aib_9 samples both left-handed and right-handed 3_{10}-helical conformations and undergoes left−right transitions on a μs time scale at room temperature (Figure 1b). This slow large-scale conformational rearrangement is found to be triggered by local residue conformational transitions on a ns time scale, which in turn are caused by ps changes of structure-stabilizing hydrogen bonds.

METHODS

Following previous work,[29] all simulations were performed with the GROMACS program suite,[35] using the GROMOS96 force field 43a1 (ref 36) to model the α-aminoisobutyric acid (Aib) peptide and the rigid all-atom model of ref 37 to describe the chloroform solvent. In variance to ref 29, we considered in this work the peptide $H_3C\text{-}CO\text{-}(NH\text{-}C_\alpha(CH_3)_2\text{-}CO)_9\text{-}CH_3$ (Aib_9) without the azobenzene photoswitch. This was done for simplicity and because the conformational dynamics of the peptide was found to virtually not depend on the presence of the photoswitch. We used a leapfrog integrator with a time step of 2 fs, the particle-mesh Ewald method for electrostatics with a minimal cutoff of 1.4 nm,[38] LINCS[39] to constrain bonds including a hydrogen atom, and the velocity rescaling algorithm[40] to run NVT simulations at 200, 220, 230, 240, 260, 280, 300, 310, 320, 330, and 350 K. For each temperature, we performed 8 production runs of 2 μs length each. To study the solvent dependence of the dynamics, at 300 K we also run simulations in SPC water.[41]

Principal component analysis (PCA) represents a linear transformation that diagonalizes the covariance matrix and thus removes the instantaneous linear correlations among the variables. To avoid possible artifacts due to the mixing of overall rotation and internal motion,[42] sine/cosine-transformed ϕ and ψ dihedral angles of the peptide backbone are used (dPCA) instead of Cartesian coordinates.[32] Figure S1 shows that the dPCA affects a time scale separation of the dynamics, where the first two principal components account for 75% of the total fluctuations.

To estimate the time scale of a transition between two conformational states A and B, we calculated the probability distribution of the first passage times of the process. The corresponding transition rate of the process is $k_{AB} = 1/2\tau_{AB}$, where τ_{AB} denotes the mean first passage time. Details on the calculation of τ_{AB} for the considered processes are given in the Supporting Information (SI).

RESULTS

Hierarchical Free Energy Landscape: Local and Global Transitions. The free energy landscape

$$\Delta G(r) = -k_B T \ln P(r) \quad (1)$$

can be calculated from a MD simulation via the probability distribution P of the molecular system along some reaction coordinate r. To identify the various processes of the Aib

DOI: 10.1021/ct501156t
J. Chem. Theory Comput. 2015, 11, 1330−1336

peptide, we therefore need to introduce appropriate (and in general multidimensional) reaction coordinates that account for the dynamics of interest. In the following, we focus on MD simulations of Aib_9 in chloroform at 300 K.

Let us first consider the slowest motions of the system, which in many cases account for its biological function. To this end, we employ a principal component analysis[31,32] on the backbone dihedral angles (see Methods and Figure S1) and consider the free energy landscape ΔG along the first two principal components V_1 and V_2 (Figure 2a). As expected from the

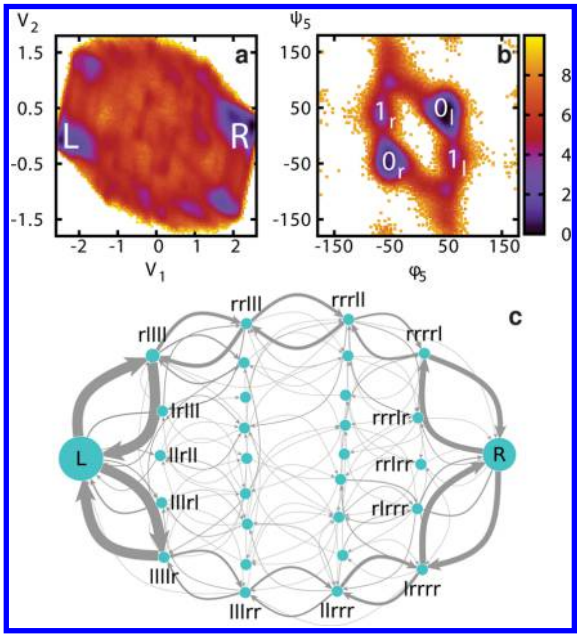

Figure 2. Calculated hierarchical free energy landscape ΔG (in units of k_BT) of Aib_9 peptide at 300 K, shown at various levels of resolution. (a) The "global" energy landscape $\Delta G(V_1,V_2)$ along the first two components of a principal component analysis reveals the overall conformational distribution including the main conformational states all-left L and all-right R. (b) The Ramachandran plot $\Delta G(\phi,\psi)$ represents the "local" energy landscape, that is, the landscape for each residue. It consists of a helical ground state 0 and an excited state 1 of the left- and right-handed conformations l and r, respectively. (c) Network representation of the global energy landscape, illustrating the pathways of the conformational transitions leading from L = (lllll) to R = (rrrrr) and back. The size of the major nodes reflects their population and the size of the arrows accounts for the associated transition probabilities. For simplicity, only a few representative states are labeled.

achirality of Aib_9, we find an overall symmetry with respect to the first principal component V_1, where the two main minima correspond to the all left-handed structure L ($V_1 \approx -2$) and the all right-handed structure R ($V_1 \approx 2$). Moreover, a number of metastable intermediate states exist that constitute pathways from L to R. Containing a mixture of right-handed (r) and left-handed (l) residues, the intermediate states can uniquely be described by a product state of these chiralities. Restricting ourselves to the five inner residues of Aib_9, we obtain, for example, L = (lllll) and R = (rrrrr), as well as (rllll) if all but residue 3 show left-handed conformations. The definition facilitates a network representation of the global energy landscape (Figure 2c), where the size of the nodes reflects the population of the associated conformational states and the size of the arrows accounts for the transition probabilities between these states (see Methods). The transition network can be shown to represent a Markov state model[33,34] (see Figure S2) that reveals all possible pathways of the L ↔ R transition of Aib_9. Sequential pathways such as (lllll) → (rllll) → (rrlll) → ⋯ are found to be most likely, although virtually all transitions between two adjacent states (i.e., states that differ only by the chirality of a single residue) take place.

As a L → R transition requires that all residues of the peptide perform a l → r transition, we next consider the underlying l ↔ r transitions of the individual residues. To this end, we adopt the backbone dihedral angles ϕ_i and ψ_i of the inner residues i = 3,...,7 as reaction coordinates. As a representative example, Figure 2b shows the free energy landscape $\Delta G(\phi,\psi)$ of residue 5. The graph, often referred to as Ramachandran plot, clearly reveals a point symmetry with respect to (0,0), which shows that Aib_9 indeed samples both left-handed ($\phi \geq 0$) and right-handed ($\phi \leq 0$) conformations with similar probability. The main conformational states 0_r at $\approx (-50°, -45°)$ and 0_l at (50°, 45°) represent a right- and left-handed helix, respectively. Moreover, we find (at least) one excited conformational state for each chirality, 1_r at $\approx (-68°, 45°)$ and 1_l at (68°, −45°); see Figure S3. Hence, a residue first needs to perform a 0 → 1 transition in order to facilitate l ↔ r transitions.

Put together, Figure 2 reveals that the global energy landscape can be characterized via the chiralities of the individual residues, which in turn are described by the local landscape $\Delta G(\phi,\psi)$ of these residues. The latter exhibit for each chirality a ground state 0 and an excited state 1, which cannot be discriminated in the two-dimensional global energy landscape $\Delta G(V_1,V_2)$. These findings indicate that the Aib peptide is described by a hierarchical free energy landscape, where tier A represents the global landscape $\Delta G(V_1,V_2)$ and tier B represents the local landscape $\Delta G(\phi,\psi)$. It is interesting to note that the appearance of the local landscape in Figure 2b also directly explains the coupling between the conformational states 0 and 1 and the chiral states l and r. Being *en-route*, the excited state 1 is obviously a required intermediate state in order to facilitate a l ↔ r transition of an individual residue.

Hierarchical Dynamics: Multiple Time Scales. As explained in the Introduction, the hallmark of hierarchical dynamics is a separation of time scales of the dynamics associated with two tiers. To learn about these time scales, Figure 3 shows the time evolution of representative pieces of a MD trajectory of Aib_9 at 300 K. We again first consider the global L ↔ R transitions of the peptide. They are monitored by the first principal component V_1, which is ≈−2 and 2 in the all-left state L and the all-right state R, respectively. Figure 3a shows the time evolution of $V_1(t)$ of a representative trajectory of 2 μs length. We count on average about 10 transitions per trajectory, that is, the time scale for a full L ↔ R transition of Aib_9 is 0.2 μs at 300 K. Figure 3a also shows the cumulative dihedral angle $\phi_{sum} = \sum_{i=3}^{7} \phi_i$. Interestingly, $\phi_{sum}(t)$ is found to perfectly match the time evolution of $V_1(t)$, which lends a straightforward structural interpretation to the first principal component. Zooming into Figure 3a, we see that the various subtransitions indeed occur sequentially, as was already suggested by the transition network in Figure 2c. Nonetheless, the first passage time of the individual transitions may vary considerably (Figure S4). We now consider local transitions of an individual residue, which are well described by its backbone dihedral angles ϕ and ψ. From the energy landscape shown in

DOI: 10.1021/ct501156t
J. Chem. Theory Comput. 2015, 11, 1330−1336

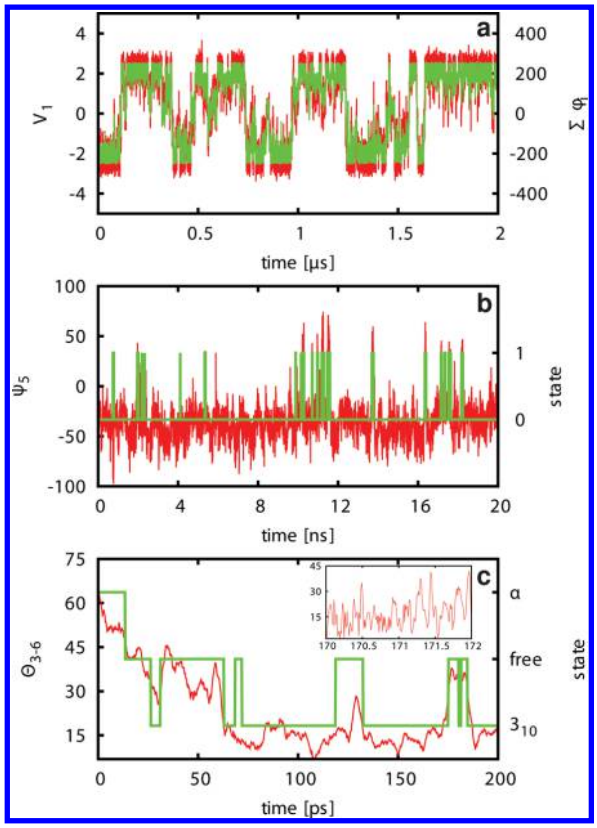

Figure 3. Structural dynamics associated with the various tiers of the hierarchical free energy landscape of Aib_9, obtained from representative pieces of a MD trajectory at 300 K. Shown is the time evolution of (a) the first principal component V_1 (red), which is virtually identical to the cumulative dihedral angle $\phi_{sum} = \sum_{i=3}^{7} \phi_i$ (green) reflecting L ↔ R transitions, (b) the backbone dihedral angle ψ_5 (red) reflecting 0 ↔ 1 transitions together with the states 0 and 1 (green), and (c) the H bond angle Θ_{3-6} (red) reflecting the making and breaking of structure-stabilizing H bonds together with the H bond states 3_{10}, α, and free (green). The inset in part c zooms in to exhibit the sub-ps fluctuations of $\Theta_{3-6}(t)$.

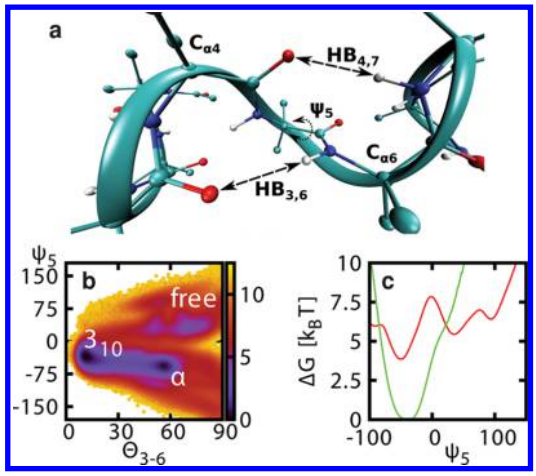

Figure 4. 4.5 mm (a) MD snapshot of the molecular structure of Aib_9 in the all-left 3_{10}-helical state, revealing the structure-stabilizing H bonds of the helix. (b) Free energy surface (in units of k_BT) at 300 K along the H bond angle Θ_{3-6} and the backbone dihedral angle ψ_5. With $\Theta_{3-6} \approx 10°$ and 60° corresponding to 3_{10}- and α-helical structures, respectively, and state 0 being located at $\psi \leq 0$ and state 1 at $\psi \geq 0$, one clearly sees that the H bond needs to be broken in order to reach the excited state 1. (c) Adiabatic free energy curves $\Delta G_b(\psi_5)$ (green line) and $\Delta G_f(\psi_5)$ (red line), corresponding to different H bonding states.

Figure 2b, we expect transitions between ground state 0 and excited state 1 of the residue, as well as transitions between the chiral states l or r. As the overall L ↔ R transitions occur in a sequential manner, the l ↔ r transitions of the middle residues (4−6) happen on a similar time scale. On the other hand, the l ↔ r transitions of end residues (1−3 and 7−9) occur much more frequently, see Figure 2c. The situation is different for the 0 ↔ 1 transitions, which can be monitored by the time evolution of the backbone dihedral angle ψ (Figure 3b). At 300 K, we count on average about 1 transition per ns. Hence, the 0 ↔ 1 transitions occur more than 2 orders of magnitude faster than the overall L ↔ R transition of the peptide.

Hydrogen Bond Dynamics Regulates Local Transitions. Just as l ↔ r transitions require a prior 0 ↔ 1 transition, 0 ↔ 1 transitions itself also require a prerequisite process, which is associated with the helix-stabilizing hydrogen (H) bonds of the peptide. To explain this, Figure 4a shows a MD snapshot of the molecular structure of Aib_9 in the all-left 3_{10}-helical state. The 3_{10}-helix is stabilized by $(n,n+3)$ -type H bonds connecting, for example, atoms O3 and HN6 (as indicated by a dashed line in Figure 4a). Restricting ourselves to the inner residues, Aib_9 may possess up to five of these H bonds. Moreover, also α-helical structures that are stabilized by $(n,n+4)$ -type H bonds may exist in Aib_9. Both α and 3_{10} helices coexist at a ratio of ≈30 to 70% for $T \geq 240$ K. As shown in Figure S5, the relative population depends on temperature.[43−45] As usual, we consider a H bond as formed, if the distance between the oxygen and nitrogen is less than 3.6 Å and if the angle Θ between the line connecting these atoms and the line connecting the O and H atom is less than 30°.

Starting in the all-left 3_{10} conformation of Aib_9, we now want to perform a 0 → 1 transition of say, residue 5. As is evident from Figure 4a, this requires the backbone dihedral angles (ϕ_5,ψ_5) around $C_{\alpha 5}$ to change from (50°, 50°) to (70°, −45°), which in turn requires the breaking of the two 3_{10}-helical H bonds on the N-terminal side of residue 5 that connect O3 and HN6 as well as O4 and HN7 (Table S1). Showing the free energy along the H bond angle Θ_{3-6} and the backbone dihedral angle ψ_5, Figure 4b illustrates this strong correlation between the existence of a H bond and the residue being in the ground state 0. To elucidate the time scale of this H bond dynamics, Figure 3c shows the time evolution of the angle Θ_{3-6}. We find multiple time scales, including sub-ps for fast structural fluctuations (see inset) that reflect ultrafast coherent H bond stretching,[46] 45 ps for the average lifetime of the 3_{10} and α helical states as well as for H bond bound-free transitions (b ↔ f), that is, the change from a H-bond stabilized helix to a structure without these H bonds. Hence we have shown that ps H bond dynamics is indeed necessary to facilitate ns (ϕ,ψ) transitions.

Hierarchy of Transition Rates. In the above analysis, we have identified a hierarchy of three dynamical processes, which correspond to three tiers in the free energy landscape illustrated in Figures 2 and 4b. Despite a time scale separation of several orders of magnitude, ps H bond breaking (b → f) was shown to be a prerequisite for ns (ϕ,ψ) conformational transitions (0 → 1), which in turn are a prerequisite for the chiral transitions (l ↔ r), that give rise to the μs global conformational rearrangement (L ↔ R) of the peptide. To

DOI: 10.1021/ct501156t
J. Chem. Theory Comput. 2015, 11, 1330−1336

study how this interscale coupling may manifest itself in measurable observables, we consider the transition rates k_α of the processes α = bf, 01, lr and LR. As Aib_9 is found to localize in a stable α-helix at low temperatures[43−45] (Figure S5), we restrict the discussion to $T \geq 240$ K. For interpretative purposes, we adopt the exponential ansatz

$$k_\alpha(T) = g_\alpha \, e^{-\Delta U_\alpha / k_B T} \tag{2}$$

where g_α denotes the constant prefactor and ΔU_α accounts for the potential energy barrier of the transition. Figure 5 shows

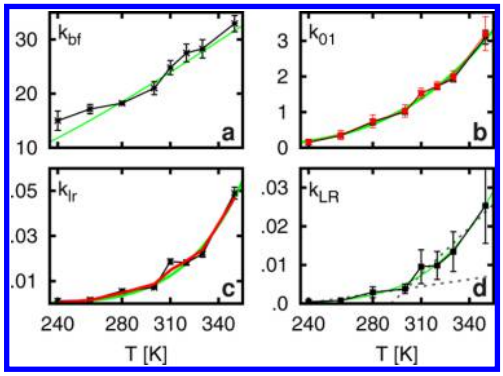

Figure 5. Temperature dependence of the transition rates k_{bf}, k_{01}, k_{lr}, and k_{LR} (in units of ns^{-1}) associated with the hierarchically coupled processes (a) H bond breaking b ↔ f, (b) (ϕ,ψ) transitions 0 ↔ 1, (c) local l ↔ r transitions, and (d) global L ↔ R transitions, respectively. Black lines are directly calculated from the MD data, green lines are fits according to the one-step process of eq 2, and red lines account for a sequential model as in eq 3. The bars in parts a−c represent the standard deviation of the mean with respect to the three inner residues, in part d they account for the variance of the mean first passage time. The biphasic behavior of $k_{LR}(T)$ in (d) is indicated by two linear fits for T < 300 K and T < 300 K.

that in all four cases the simple exponential model (green lines) matches the calculated transition rates $k_\alpha(T)$ (black lines, see Methods) quite well. For example, the b ↔ f transitions of the H bonds can be modeled by a prefactor $1/g_{bf}$ = 3.7 ps and a barrier height $\Delta U_{bf} = 2.5 k_B T_0$ (T_0 = 300 K), which results in a time scale of 45 ps at 300 K (cf. Figure 3 c).

The 0 ↔ 1 transition in the (ϕ,ψ) energy landscape results in a prefactor $1/g_{01}$ = 0.7 ps and a barrier height of ΔU_{01} = 7.1 $k_B T_0$, which corresponds to a time scale of 1 ns at 300 K (Figure 5b). Following the discussion above, however, the interpretation of the 0 → 1 transition as a one-step process, $(b, 0) \overset{k_{01}}{\rightarrow} (f, 1)$, appears misleading. To account for the fact that first the breaking of H bonds is required, we consider the sequential process

$$(b, 0) \underset{k_{fb}}{\overset{k_{bf}}{\rightleftharpoons}} (f, 0) \overset{k'_{01}}{\rightarrow} (f, 1) \tag{3}$$

where the "direct" rate k'_{01} is generally larger than the "overall" rate k_{01}. When we assume that $k_{bf}, k_{fb} \gg k'_{01}$, the coupled rate equation associated with eq 3 is readily solved to give

$$k_{01}(T) = k_{bf}(T) \, \frac{k'_{01}(T)}{k_{fb}(T)} \tag{4}$$

Figure 5b shows that results from this sequential model are in excellent agreement with the MD data and also reproduce nonexponential features of k_{01}(T) such as the "hump" from 300 to 330 K. Hence the simple expression eq 4 can explain the coupling between fast b ↔ f transitions and slow 0 ↔ 1 transitions. The first step is described by the H-bond opening rate $k_{bf}(T)$, thereby introducing the temperature dependence of the underlying fast process. The competition between the two possible subsequent processes is described in eq 4 by the ratio of the direct rate k'_{01} and the H-bond closing rate k_{fb}. Given that the back-rate ($1/k_{fb}$ = 10 ps) is clearly larger than the forward-rate ($1/k'_{01}$= 200 ps) (cf. Figure S6), the observed time scale separation between b → f and 0 → 1 transitions is a consequence of a sequential reaction with a high back-rate rather than caused by different barrier heights. The two scenarios are illustrated by dotted and full lines in Figure 1a.

Similarly, we can express the rate k_{lr} either by a one-step process (giving $\Delta U_{lr} = 10.7 k_B T_0$) or by a sequential process, which is proportional to the rate k_{01}(T) of the underlying fast process (Figure 5c). Again the back-rate ($1/k_{10}$= 10 ps) is clearly faster than the forward-rate ($1/k'_{lr}$ = 200 ps, Figure S6), thus resulting in a time scale separation between 0 ↔ 1 and l ↔ r transitions. Finally, consisting of a succession of local l ↔ r transitions, the L ↔ R transition occurs with a rate $k_{LR}(T)$ (Figure 5d), whose temperature behavior is quite similar to the one of $k_{lr}(T)$.

The transition rates shown in Figure 5 report on the temperature induced onset of the corresponding dynamics.[47] As a consequence of the hierarchical coupling between the various processes, the temperature behavior is quite similar in all four cases and becomes more pronounced for the higher tiers. As indicated by two linear fits in Figure 5d, the rise of $k_{LR}(T)$ may be considered as biphasic for T < 300 K and T > 300 K, and therefore be interpreted as a dynamic transition with a transition temperature of ≈300 K. We note that the dynamic transition of Aib_9 in chloroform is of intramolecular origin rather than driven by the solvent. A prominent example for the latter case is the well-established dynamic transition of proteins in water, which is associated with the glass transition of solvent water at ≈220 K.[48−51] While the water glass transition can be clearly deduced from the biphasic temperature dependence of the diffusion constant,[51] no such effect is seen for chloroform (Figure S7) in the entire considered temperature range 200−350 K.

DISCUSSION AND CONCLUSIONS

To summarize, we have performed extensive MD simulations (≈200 μs) of a small peptide followed by dimensionality reduction analysis. Adopting the achiral peptide Aib_9 as a simple but nontrivial model system, we have discovered a hierarchy of (at least) three tiers of the molecule's free energy landscape (Figure 2), corresponding to (A) chiral left- to right-handed transitions (L ↔ R) of the entire peptide which take about 0.2 μs to complete, (B) conformational (ϕ,ψ) transitions (0 ↔ 1) of individual residues on a 1 ns time scale, and (C) the opening and closing of structure-stabilizing H bonds (b ↔ f) occurring within tens of ps, which are triggered by sub-ps structural fluctuations. Despite a time scale separation of in total 6 orders of magnitude (Figure 3), ps H bonding was shown to be a prerequisite for the ns (ϕ,ψ) conformational dynamics, which in turn was found to be a prerequisite for the μs global conformational rearrangement of the peptide. We have shown that the time scale separation between the various processes can be explained by sequential reactions with relatively high back-rates but roughly similar transition rates in forward direction. Yielding a similar temperature behavior of

DOI: 10.1021/ct501156t
J. Chem. Theory Comput. 2015, 11, 1330−1336

all considered processes, the hierarchical mechanism results in a dynamic transition of Aib_9 at ≈300 K. Let us finally point out some interesting conclusions arising from these results. To begin, we would like to stress that, unlike to the popular "artist's view" in Figure 1a, the true free energy landscape and dynamics of even a small peptide is intrinsically multidimensional. To extract the few functionally relevant motions from a 3*N*-dimensional MD trajectory, systematic dimensionality reduction techniques such as principal component analysis (PCA) are required, which may define appropriate reaction coordinates for the various types of motion. In line with previous studies,[32,42] we have found that internal angular coordinates are of advantage, including the H bonding angle Θ (Figure 4) to describe the opening and closing of structure-stabilizing H bonds, the Ramachandran angle ψ to account for the 0 ↔ 1 transitions of the individual residues (Figure 2b), and the first two principal components of an analysis using the peptide's backbone dihedral angles, which was shown to directly build up a network of L ↔ R transitions including all their pathways and intermediate states (Figure 2c).

Next, we return to our original question which dynamic transition was probed by the transient infrared spectra of Hamm and co-workers.[25−27] As these experiments do not discriminate the chirality of the peptide, they cannot observe the chiral transitions l ↔ r and L ↔ R. Moreover, even the fastest process discussed above (the H bond opening within ≈45 ps) appears too slow to cause the observed effects of the infrared spectra. It should be stressed, however, that the reaction coordinates describing the above-discussed dynamic transition are not necessarily equivalent to the 'spectroscopic coordinates' accounting, for example, for the measured frequency distribution of the C═O vibrations. In fact, when we apply a previously developed model of amide I spectroscopy to Aib_9,[52] we find that the modulation of the C═O frequency is significantly stronger in the conformationally excited state 1 than in the corresponding ground state 0.[29] That is, although the 0 ↔ 1 transitions (corresponding to tier B) occur on a ns time scale, they switch between two different energy landscapes (corresponding to tier C), which exhibit different sub-ps fluctuations of the C═O frequency.

Lastly, it is instructive to describe the hierarchical coupling between fast and slow degrees of freedom in terms of a representation that allows us to connect the multiscale dynamics with the theory of nonadiabatic transitions.[53] Adopting the H bond-(ϕ,ψ) coupling as an example, Figure 4c shows one-dimensional free energy curves of the bound state $\Delta G_b(\psi_5)$ and the free state $\Delta G_f(\psi_5)$, whose calculations use only MD frames with and without 3−6 H bond, respectively. $\Delta G_b(\psi_5)$ exhibits a single minimum corresponding to the motion of ψ_5 confined in state 0. On the other hand, $\Delta f_b(\psi_5)$ shows several minima connected via small barriers, revealing the possibility of 0 ↔ 1 transitions. It is interesting to note the direct analogy of this representation with the common adiabatic picture of electronic potential-energy curves $V_n(x)$, where n = 0,1,... labels the electronic state and x represents a nuclear coordinate. In this view, $\Delta G_b(\psi_5)$ and $\Delta G_f(\psi_5)$ represent *adiabatic* free energy curves corresponding to different H bonding states, and changes between these states correspond to *nonadiabatic* transitions.

While the present case study has focused on a small peptide, we speculate that the basic hierarchical mechanism—breaking of H bonds facilitates local conformational which trigger a global conformational rearrangement—is much more general and may also apply, for example, to refolding processes of proteins and RNA.

■ ASSOCIATED CONTENT

Supporting Information

Dihedral angle principal component analysis (Figure S1), Markovianity of global transition network (Figure S2), definition of conformational states (Figure S3), mean first passage time distributions (Figure S4), Correlation between H bonding and (0 ↔ 1) conformational transitions (Table S1), Coexistence of α- and 3_{10}-helical structures (Figure S5), sequential model (Figure S6), and effect of solvent (Figure S7). This material is available free of charge via the Internet at http://pubs.acs.org.

■ AUTHOR INFORMATION

Corresponding Author

*Phone: +49 761 2035750. E-mail: stock@physik.uni-freiburg.de.

Notes

The authors declare no competing financial interest.

■ ACKNOWLEDGMENTS

We thank Peter Hamm, Claudio Toniolo, Tran Thanh Thuy, and Maja Kobus for numerous instructive and helpful discussions. This work has been supported by the Deutsche Forschungsgemeinschaft.

■ REFERENCES

(1) Pesenson, M. Z. *Multiscale Analysis and Nonlinear Dynamics*; Wiley-VCH: Weinheim, 2013.
(2) Berendsen, H. J. C. *Simulating the Physical World*; University Press: Cambridge, 2007.
(3) Henzler-Wildman, K.; Kern, D. Dynamic personalities of proteins. *Nature (London)* **2007**, *450*, 964−972.
(4) Lange, O. F.; Lakomek, N.-A.; Schröder, G. F.; Walter, K. F. A.; Becker, S.; Meiler, J.; Grubmüller, H.; Griesinger, C.; de Groot, B. L. Recognition dynamics up to microseconds revealed from an RDC-derived ubiquitin ensemble in solution. *Science* **2008**, *320*, 1471−1475.
(5) Smock, R. G.; Gierasch, L. M. Sending signals dynamically. *Science* **2009**, *324*, 198−203.
(6) Leitner, D.; Straub, J. *Proteins: Energy, Heat and Signal Flow*; Taylor and Francis CRC Press: London, 2009.
(7) Hensen, U.; Meyer, T.; Haas, J.; Rex, R.; Vriend, G.; Grubmüller, H. Exploring protein dynamics space: The dynasome as the missing link between protein structure and function. *PLoS One* **2012**, *7*, e33931.
(8) Cui, Q., Bahar, I. *Normal Mode Analysis*; Chapman & Hall: London, 2006.
(9) van Gunsteren, W. F.; Karplus, M. Effect of contraints on the dynamics of macromolecules. *Macromolecules* **1982**, *15*, 1528−1544.
(10) Ermak, D. L.; McCammon, J. A. Brownian dynamics with hydrodynamic interactions. *J. Chem. Phys.* **1978**, *69*, 1352−1360.
(11) Depa, P.; Chen, C.; Maranas, J. K. Why are coarse-grained force fields too fast? A look at dynamics of four coarse-grained polymers. *J. Chem. Phys.* **2011**, *134*, 014903.
(12) Henzler-Wildman, K. A.; Lei, M.; Thai, V.; Kerns, S. J.; Karplus, M.; Kern, D. A hierarchy of timescales in protein dynamics is linked to enzyme catalysis. *Nature (London)* **2007**, *450*, 913−916.
(13) Fuentes, E. J.; Gilmore, S. A.; Mauldin, R. V.; Lee, A. L. Evaluation of energetic and dynamic coupling networks in a PDZ domain protein. *J. Mol. Biol.* **2006**, *364*, 337−351.
(14) Frauenfelder, H.; Sligar, S.; Wolynes, P. The energy landscapes and motions of proteins. *Science* **1991**, *254*, 1598−1603.

DOI: 10.1021/ct501156t
J. Chem. Theory Comput. 2015, 11, 1330−1336

(15) Metzler, R.; Klafter, J.; Jortner, J. Hierarchies and logarithmic oscillations in the temporal relaxation patterns of proteins and other complex systems. *Proc. Natl. Acad. Sci. U.S.A.* **1999**, *96*, 11085−11089.
(16) Maisuradze, G. G.; Liwo, A.; Senet, P.; Scheraga, H. A. Local vs global motions in protein folding. *J. Chem. Theory Comput.* **2013**, *9*, 2907−2921.
(17) Ball, K. D.; Berry, R. S.; Kunz, R. E.; Li, F.-Y.; Proykova, A.; Wales, D. J. From topographies to dynamics on multidimensional potential energy surfaces. *Science* **1996**, *271*, 963−965.
(18) Onuchic, J. N.; Schulten, Z. L.; Wolynes, P. G. Theory of protein folding: The energy landscape perspective. *Annu. Rev. Phys. Chem.* **1997**, *48*, 545−600.
(19) Dill, K. A.; Chan, H. S. From Levinthal to pathways to funnels: The "new view" of protein folding kinetics. *Nat. Struct. Biol.* **1997**, *4*, 10−19.
(20) Bicout, D. J.; Szabo, A. Entropic barriers, transitions states, funnels, and exponential protein folding kinetics: A simple model. *Protein Sci.* **2000**, *9*, 452−465.
(21) Gruebele, M. Protein folding: The free energy surface. *Curr. Opin. Struct. Biol.* **2002**, *12*, 161−168.
(22) Wales, D. J. *Energy Landscapes*; Cambridge University Press: Cambridge, 2003.
(23) Miyashita, O.; Wolynes, P. G.; Onuchic, J. N. Simple energy model for the kinetics of functional transitions in proteins. *J. Phys. Chem. B* **2005**, *109*, 1959−1969.
(24) Best, R. B.; Hummer, G. Coordimate-dependent diffusion in protein folding. *Proc. Natl. Acad. Sci. U.S.A.* **2010**, *107*, 1088−1093.
(25) Botan, V.; Backus, E.; Pfister, R.; Moretto, A.; Crisma, M.; Toniolo, C.; Nguyen, P. H.; Stock, G.; Hamm, P. Energy transport in peptide helices. *Proc. Natl. Acad. Sci. U.S.A.* **2007**, *104*, 12749−12754.
(26) Backus, E.; Nguyen, P. H.; Botan, V.; Pfister, R.; Moretto, A.; Crisma, M.; Toniolo, C.; Stock, G.; Hamm, P. Structural flexibility of a helical peptide regulates vibrational energy transport properties. *J. Phys. Chem. B* **2008**, *112*, 15487−15492.
(27) Backus, E. H. G.; Bloem, R.; Pfister, R.; Moretto, A.; Crisma, M.; Toniolo, C.; Hamm, P. Dynamical transition in a small helical peptide and its implication for vibrational energy transport. *J. Phys. Chem. B* **2009**, *113*, 13405−13409.
(28) Nguyen, P. H.; Park, S. M.; Stock, G. Nonequilibrium molecular dynamics simulation of the energy transport through a peptide helix. *J. Chem. Phys.* **2010**, *132*, 025102.
(29) Kobus, M.; Nguyen, P. H.; Stock, G. Infrared signatures of the peptide dynamical transition: A molecular dynamics simulation study. *J. Chem. Phys.* **2010**, *133*, 034512.
(30) Rohrdanz, M. A.; Zheng, W.; Clementi, C. Discovering mountain passes via torchlight: Methods for the definition of reaction coordinates and pathways in complex macromolecular reactions. *Annu. Rev. Phys. Chem.* **2013**, *64*, 295−316.
(31) Amadei, A.; Linssen, A. B. M.; Berendsen, H. J. C. Essential dynamics of proteins. *Proteins* **1993**, *17*, 412−425.
(32) Altis, A.; Otten, M.; Nguyen, P. H.; Hegger, R.; Stock, G. Construction of the free energy landscape of biomolecules via dihedral angle principal component analysis. *J. Chem. Phys.* **2008**, *128*, 245102.
(33) Rao, F.; Caflisch, A. The protein folding network. *J. Mol. Biol.* **2004**, *342*, 299−306.
(34) Noe, F.; Horenko, I.; Schütte, C.; Smith, J. C. Hierarchical analysis of conformational dynamics in biomolecules: Transition networks of metastable states. *J. Chem. Phys.* **2007**, *126*, 155102.
(35) van der Spoel, D.; Lindahl, E.; Hess, B.; Groenhof, G.; Mark, A. E.; Berendsen, H. J. C. Gromacs; Fast, flexible, and free. *J. Comput. Chem.* **2005**, *26*, 1701−1718.
(36) van Gunsteren, W. F.; Billeter, S. R.; Eising, A. A.; Hünenberger, P. H.; Krüger, P.; Mark, A. E.; Scott, W. R. P.; Tironi, I. G. *Biomolecular Simulation: The GROMOS96 Manual and User Guide*; Vdf Hochschulverlag AG an der ETH Zürich: Zürich, 1996.
(37) Tironi, I. G.; van Gunsteren, W. F. A molecular dynamics simulation study of chloroform. *Mol. Phys.* **1994**, *83*, 381.
(38) Darden, T.; York, D.; Petersen, L. Particle mesh Ewald: An N log(N) method for Ewald sums in large systems. *J. Chem. Phys.* **1993**, *98*, 10089.
(39) Hess, B.; Bekker, H.; Berendsen, H. J. C.; Fraaije, J. G. E. M. LINCS: A linear constraint solver for molecular simulations. *J. Comput. Chem.* **1997**, *18*, 1463−1472.
(40) Bussi, G.; Donadio, D.; Parrinello, M. Canonical sampling through velocity rescaling. *J. Chem. Phys.* **2007**, *126*, 0141011−0141017.
(41) Berendsen, H. J. C.; Postma, J. P. M.; van Gunsteren, W. F.; Hermans, J. In *Intermolecular Forces*; Pullman, B., Ed.; D. Reidel Publishing Company: Dordrecht, 1981; pp 331−342.
(42) Sittel, F.; Jain, A.; Stock, G. Principal component analysis of molecular dynamics: On the use of Cartesian vs internal coordinates. *J. Chem. Phys.* **2014**, *141*, 014111.
(43) Hummel, R.-P.; Toniolo, C.; Jung, G. Conformational transitions between enantiomeric 3_{10}-helices. *Angew. Chem., Int. Ed. Engl.* **1987**, *26*, 1150−1152.
(44) Smythe, M. L.; Huston, S. E.; Marshall, G. R. The molten helix: Effects of solvation on the α- to 3_{10}-helical transition. *J. Am. Chem. Soc.* **1995**, *117*, 5445−5452.
(45) Banerjee, R.; Chattopadhyay, S.; Basu, G. Conformational preferences of a short Aib/Ala-based water-soluble peptide as a function of temperature. *Proteins* **2009**, *76*, 184−200.
(46) Madsen, D.; Stenger, J.; Dreyer, J.; Nibbering, E. J.; Hamm, P.; Elsaesser, T. Coherent vibrational ground-state dynamics of an intramolecular hydrogen bond. *Chem. Phys. Lett.* **2001**, *341*, 56−62.
(47) Tang, K. E. S.; Dill, K. A. Native protein fluctuations: The conformational-motion temperature and the inverse correlation of protein flexibility with protein stability. *J. Biomol. Struct. Dyn.* **1998**, *16*, 397−411.
(48) Doster, W.; Cusack, S.; Petry, W. Dynamical transition of myoglobin revealed by inelastic neutron scattering. *Nature* **1989**, *337*, 754−756.
(49) Ansari, A.; Jones, C. M.; Henry, E. R.; Hofrichter, J.; Eaton, W. A. The role of solvent viscosity in the dynamics of protein conformational changes. *Science* **1992**, *256*, 1796−1798.
(50) Vitkup, D.; Ringe, D.; Petsko, G. A.; Karplus, M. Solvent mobility and the protein 'glass' transition. *Nat. Struct. Biol.* **2000**, *7*, 34−38.
(51) Tournier, A. L.; Xu, J.; Smith, J. C. Translational hydration water dynamics drives the protein glass transition. *Biophys. J.* **2003**, *85*, 1871−1875.
(52) Gorbunov, R. D.; Kosov, D. S.; Stock, G. Ab initio-based exciton model of amide I vibrations in peptides: Definition, conformational dependence, and transferability. *J. Chem. Phys.* **2005**, *122*, 224904.
(53) Domcke, W., Yarkony, D. R., Köppel, H. *Conical Intersections: Electronic Structure, Dynamics, and Spectroscopy*; World Scientific: Singapore, 2004.

DOI: 10.1021/ct501156t
J. Chem. Theory Comput. 2015, 11, 1330−1336